ACS APPLIED MATERIALS & INTERFACES

Research Article

www.acsami.org

Red, Yellow, and Blue Luminescence by Graphene Quantum Dots: Syntheses, Mechanism, and Cellular Imaging

Tian Gao,[†] Xi Wang,[†] Li-Yun Yang,[†] Huan He,[†] Xiao-Xu Ba,[†] Jie Zhao,[†] Feng-Lei Jiang,*[,†] and Yi Liu*[,†,‡,§]

[†]State Key Laboratory of Virology & Key Laboratory of Analytical Chemistry for Biology and Medicine, College of Chemistry and Molecular Sciences, Wuhan University, Wuhan 430072, P. R. China

[‡]School of Chemistry and Chemical Engineering, Wuhan University of Science and Technology, Wuhan 430081, P. R. China

[§]College of Chemistry and Material Science, Guangxi Teachers Education University, Nanning 530001, P. R. China

Supporting Information

ABSTRACT: Owing to their excellent photoluminescence (PL) properties, good biocompatibility, and low toxicity, graphene quantum dots (GQDs) are widely applied in bioimaging, biosensing, and so forth. However, further development of GQDs is limited by their synthetic methodology and unclear PL mechanism. Therefore, it is urgent to find efficient and universal methods for the synthesis of GQDs with high stability, controllable surface properties, and tunable PL emission wavelength. By coating with polyethyleneimine (PEI) of different molecular weights, blue-, yellow-, and red-emitting GQDs were successfully prepared. By transmission electron microscopy, atomic force microscopy, and dynamic light scattering, the characterization of size and morphology revealed that blue-emitting PEI_{1800} GQDs were monocoated, like jelly beans, and red-emitting PEI_{600} GQDs were multicoated, like capsules. The amidation reaction between carboxyl and amide functional groups played an important role in the coating process, as evidenced by IR spectroscopy and theoretical calculation with density functional theory B3LYP/6-31G*. The PL-tunable GQDs exhibited an excellent chemical stability and extremely low cytotoxicity, and they had been shown to be feasible for bioimaging, making these GQDs highly attractive for a wide variety of applications, including multicolor imaging and bioanalysis.

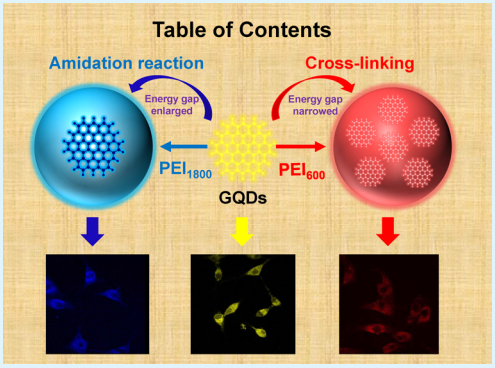

KEYWORDS: *Graphene quantum dots, polyethyleneimine, photoluminescence tunable, coating nanomaterials, photoluminescence mechanism, cellular imaging*

1. INTRODUCTION

Graphene quantum dots (GQDs) show great potential in the fields of photoelectronics, photovoltaics,[1,2] biosensing,[3] and bioimaging[4] owing to their unique photoluminescence (PL) properties, including excellent biocompatibility, low toxicity,[5] and high stability against photobleaching and photoblinking.[6] Typically, GQDs possess a mono- or multiple-layered graphite core, with chemical groups on the edge. Unlike pristine graphene, which does not emit in the visible light region,[7,8] GQDs have a suitable band gap for visible light emissions due to their structural defects, elementary composition, and surface groups.[9−12] Considerable research efforts have been devoted to exploring different kinds of synthetic methods, which can be sorted into top-down nano cutting methods and bottom-up organic approaches.[13,14] Top-down methods were widely used to prepare GQDs for their cheap raw materials, simple synthetic routes, and normal reaction conditions. Varieties of carbon resources with an sp^2 carbon structure, like graphene oxide, carbon fiber, carbon nanotubes, and carbon black, can be used as raw materials to get GQDs by cutting with acid oxidization, hydrothermal, or electrochemical methods.[15] It is worthwhile mentioning that single-layer GQDs could be obtained by "one-pot" acid oxidizing synthetic method by cutting carbon black, which is easily available and low in cost.[16] This work is creative and important to expand the applications and scale of production of GQDs.

Now, there are still two vital challenges for better application of GQDs, namely (i) designing universal synthetic methods for tunable PL and (ii) understanding the exact PL mechanism of GQDs by controlling the structure. To expand the possible applications of these PL materials, it is highly desirable to develop a strategy to tune their PL properties. Indeed, single color detection and imaging are unattractive for most applications due to their low signal to noise ratio. However, multichannel detection and multicolor imaging have high signal to noise ratios because the background results from a low bandwidth interference. Thus, a tunable emission maximum is especially important for GQDs because it enables these

Received: April 20, 2017
Accepted: July 5, 2017
Published: July 5, 2017

DOI: 10.1021/acsami.7b05569
ACS Appl. Mater. Interfaces XXXX, XXX, XXX−XXX

materials to be used for multichannel detection and multicolor imaging. Furthermore, various emission colors can be obtained by well adjusting PL-tunable materials, thus showing an even greater potential in imaging and quantum dot light-emitting diodes.[17,18] Previous reports have shown that the peak emission wavelength of GQDs shifts with changing excitation wavelength. The shifted PL intensity sharply decreases as the excitation wavelength moves away from the peak wavelength of the GQDs' absorbance. This kind of excitation-dependent emission could not be truly labeled as "tunable" because the shifted PL intensity is so small that it is inadequate for real biomedical applications.[19] Researchers have done much work on PL-tunable GQDs. Especially, Tetsuka's group pioneered to prepare amino-functionalized GQDs to tune the emitting color from blue to yellow and Tseng's group obtained four kinds of color-emitting GQDs by using ammonium hydroxide and thiourea to control synthetic conditions and applied them in bioimaging.[10,20] Recently, Wanunu's group creatively synthesized PL-tunable GQDs from blue to yellow by peptide decoration and explored further functionalization with DNA.[21] However, until now only few PL-tunable synthetic methods are reported, which are still far from adequate for GQDs to be widely applied. Therefore, it is urgent to develop novel methods to synthesize GQDs with tunable PL covering the entire visible spectrum.

To engineer the PL properties of GQDs, we must first elucidate the PL mechanism.[14,22−24] Only by understanding the PL mechanism completely, can we really design truly "tunable" GQDs. Graphene shows quantum confinement effects because of the infinite Bohr diameter of excitons.[25] Thus, GQDs exhibit a nonzero band gap and fluorescence upon excitation.[26−28] This band gap could be influenced by various factors. For example, in recent years, researchers speculated that the particle size, edge state, element content, and type of functional group were the most critical factors affecting the PL mechanism of GQDs.[29−32] These factors are inevitably convoluted with each other; thus, in a given system, the effects of each of these factors are difficult to determine. Therefore, isolating the effects of a single factor when devising a one-step synthetic method are incredibly difficult because most changes to the method affect multiple critical factors. For example, when trying to modify the surface of GQDs from the beginning, it is hard to keep both the carbon-bone structure and the size of inner graphene unchanged. Therefore, it is worthwhile to attempt to find a universal method to change the PL properties of GQDs by one step further treatment. The coating reaction for GQDs is exactly one of the choices to fulfill the requirements. By coating GQDs with materials, it is easy to form a core−shell structure to protect the inner original nanographene core and have a passivation effect to make it more stable. At the same time, coating materials have a potential to change PL properties of GQDs to implement multiple color syntheses.

In previous studies, polymers, such as polydopamine,[33] poly(ethylene glycol) (PEG),[13,34] and polyvinyl pyrrolidone (PVP),[35] have already been employed as coating materials to improve PL properties of carbon nanodots (CNDs) and GQDs. Coating GQDs with these polymers results in surface functionalization, surface passivation, and enhancement of quantum yields (QYs) of GQDs. However, previously these coating materials were rarely shown to enable tunable PL emission.[36] Polyethyleneimine (PEI) is a typical positive-charged polymer, with rich amino groups, which is widely used in gene and drug delivery. Researchers also designed PEI/CNDs core−shell structures as nano probes, DNA visual deliverers, and biosensors.[31,37] PEI is a nitrogenous polymer, which has great potential to modify GQDs by tuning their PL properties and make it possible to do multicolor imaging due to their excellent biocompatibility. In addition, because the PL mechanism of coated GQDs is seldom investigated, we do not understand how these coatings may affect the PL mechanism. Hence, it is desirable to devise both experimental and theoretical methods to study the PL mechanism of polymer-coated GQDs.

In this work, yellow-emitting bare GQDs were prepared from carbon black. Blue-emitting PEI_{1800} GQDs and red-emitting PEI_{600} GQDs were obtained by coating with PEI of different molecular weights. The structures of PEI-coated GQDs were investigated by a series of characterization methods. Moreover, a theoretical study with density functional theory (DFT) B3LYP/6-31G* was used to obtain the energy gap and charge density.[38] Then, PL mechanisms of PEI-coated GQDs were discussed by combining both the experimental and theoretical results. After evaluation of their stability and biocompatibility, these GQDs were applied in cellular imaging.

2. EXPERIMENTAL SECTION

2.1. Chemicals and Instruments. Carbon Black VXC-72 was purchased from Cabot Corporation (Boston, MA). PEI with molecular weight of 600 and 1800 Da was purchased from Aladdin (Shanghai, China). Nitric acid (HNO_3), disodium hydrogen phosphate (Na_2HPO_4), potassium dihydrogen phosphate (KH_2PO_4), sodium chloride (NaCl), potassium chloride (KCl), dimethyl sulfoxide (DMSO), quinine sulfate, Rhodamine B, 3-(4,5-dimethyldiazol-2-yl)-2,5-diphenyltetrazolium bromide (MTT), and fetal bovine serum (FBS) were purchased from Sigma (St. Louis, MO). All chemicals were of analytical grade and were used as received. All solutions were prepared with deionized (DI) water from the Mill-Q-RO4 water purification system (Millipore).

Fluorescence analysis was carried out on an LS-55 fluorophotometer (Perkin-Elmer). Absorption spectra were recorded by a UNICO 4802 UV−vis double-beam spectrophotometer. High-resolution transmission electron microscopy (HRTEM) images were obtained on a JEM-2100 (JEOL, Japan) electron microscope operating at 200 kV. Atomic force microscopy (AFM) images were obtained on an Ntegra Spectra AFM microscope (NT-MDTN, Russia) with tapping mode. Fourier transform infrared (FTIR) spectra were obtained on a Thermo FTIR spectrophotometer. X-ray photoelectron spectra (XPS) were recorded with a KRATOS XSAM800 X-ray photoelectron spectrometer (Kratos Analytical Ltd, Manchester), using Mg as the exciting source. Ultrasonic treatment was carried out on a SCIENTZ-II D ultrasonic cell crusher (Ningbo Scientz Biotechnology Co., Ltd) at 950 W. Powder X-ray diffraction (PXRD) spectra were obtained on PANalytical B.V. (Netherlands) X'PERT PXRD. Dynamic light scattering (DLS) was tested on a ZEN 3600 (Malvern Instruments, U.K.) DLS instrument. Zeta potential data were also measured on a ZEN 3600 Zetasizer analyzer (Malvern Instruments, U.K.). Time-resolved fluorescence spectra were recorded via QM4CW/Q11A steady state spectrofluorometer systems (PTI). Cell imaging was done on a Perkin-Elmer Ultraview Vox confocal microscope (MA). All calculations were optimized with DFT (DFT-B3LYP/6-31+G*) methods,[39] using the Gaussian 09 program (Gaussian Inc., Wallingford CT, 2009).

2.2. Syntheses of GQDs. GQDs were synthesized by a low-temperature pyrolysis of VCX-72 carbon black in nitric acid. In a typical procedure, 0.4 g of dried VCX-72 carbon black was refluxed in 100 mL of HNO_3 (6 mol L^{-1}) for 24 h. The suspension, after cooling to room temperature, was treated by an ultrasonic cell crusher for 10 min at 950 W and then centrifuged (8000 rpm) for 10 min to obtain the supernatant. The supernatant was filtered through a 0.22 μm micromembrane filter (Millipore). Rotary evaporation was used to

DOI: 10.1021/acsami.7b05569
ACS Appl. Mater. Interfaces XXXX, XXX, XXX−XXX

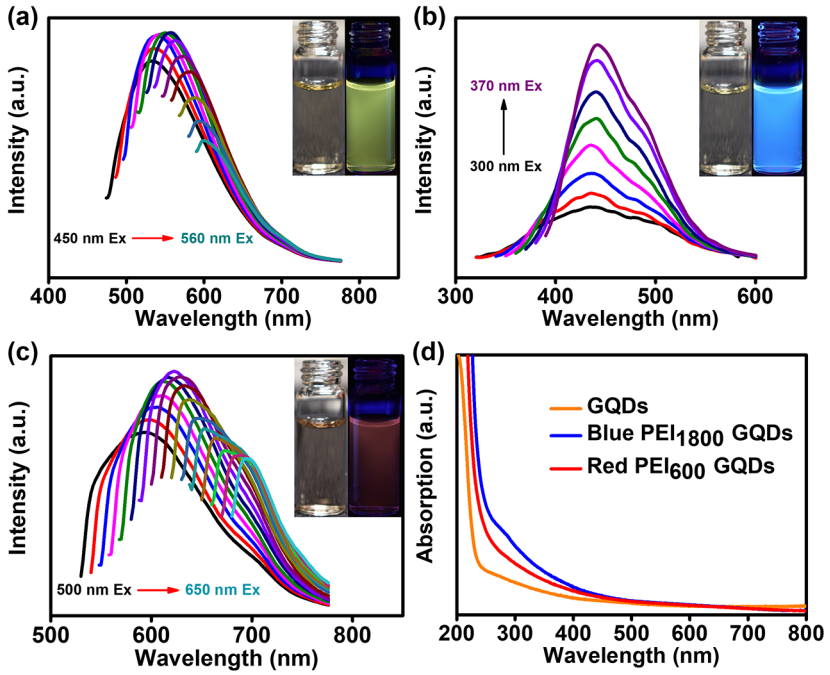

Figure 1. PL spectra of GQDs (a), PEI_{1800} GQDs (b), and PEI_{600} GQDs (c) at different excitation wavelengths. Inset: photograph of aqueous solution of these three GQDs under room light (left) and 365 nm UV irradiation lamp (right). UV−vis absorption spectra (d) of GQDs, PEI_{1800} GQDs, and PEI_{600} GQDs dispersed in water.

remove the acid. The dried sample was dissolved in 10 mL of DI water and then dialyzed in 3500 Da dialysis bag for 1 day. Furthermore, freeze-drying (lyophilization) was utilized to obtain the GQD powder.

2.3. Syntheses of PEI-Coated GQDs. To find the optimal reaction condition, different reagent dosages and reaction times were tested. One typical synthetic strategy is shown in Figure S1. After 50 mg of GQDs were redissolved in 20 mL of ultrapure water, a portion of PEI was added into the solution and the mixture was heated to the boiling temperature. When a gel was formed, 10 mL of ultrapure water was added to prevent it from drying and scorching. This procedure was repeated three times to get PEI-coated GQDs. Ultrapure water was added to bring the total volume up to 10 mL. After extraction by ethanol (GQDs are insoluble in ethanol, whereas PEI is soluble) and dialysis in a 3000 Da dialysis bag for 24 h, pure PEI-coated GQDs were obtained. PEI with a different molecular weight was used to obtain GQDs with tunable PL properties. A solid powder of the GQDs was obtained by freeze-drying. Photos of GQDs and PEI-coated GQD powder are shown in Figure S2.

2.4. Cell Culture. The human embryonic kidney cell line 293 (HEK-293) and human primary glioblastoma cell line 87 (U-87) cells were cultured in Dulbecco's modified Eagle's medium (DMEM) supplemented with 10% FBS, 1% penicillin, and 1% amphotericin at 37 °C in 5% CO_2.

2.5. Cell Viability. For the MTT assay, HEK-293 and U-87 cells were used to evaluate the biocompatibility of the obtained PEI_{1800} GQDs, uncoated GQDs, and PEI_{600} GQDs. A 200 μL suspension of the two kinds of cells in the exponential growth phase were seeded into each well of a 96-well plate at a density of 1×10^4 per well. After being cultured for 12 h, GQDs with different concentrations were co-cultured with the cells for 24 h. Cells cultured without GQDs were taken as a control. After incubation, the cells were washed with phosphate-buffered saline (PBS). A 5 mg mL^{-1} MTT reagent was added into each well and incubated at 37 °C for 4 h until the emergence of a purple precipitate. Then, the medium was removed and 150 μL DMSO was added. To dissolve the crystals completely, the suspension was vibrated for 15 min. Finally, the optical density of each well at 490 nm was recorded on an Elx800 Micropalte reader (BioTek). In addition, blank group wells were added with the medium and MTT solution without cells. To accurately measure the viability of each test group, six replicate wells were used and all of the experiments were repeated at least three times. The results were exhibited as the mean ± standard deviation. The cell viability was calculated by the following equation

$$\text{cell viability } \% = (OD_{samples} - OD_{blank})/(OD_{control} - OD_{blank}) \times 100\%$$

2.6. Cell Imaging. U-87 cells in the exponential phase were seeded into 6-well plates with aseptic coverslips at a concentration of 1×10^6 cells per well. These cells were cultured at 37 °C for 24 h, using 5% CO_2 for cell attachment. PEI_{1800} GQD, GQD, and PEI_{600} GQD (after being filtered with a 0.22 μm PES membrane) solution, with a concentration of 50 μg/mL in the culture medium, were added into the U-87 cells to replace the original medium. After growing for 18 h, PBS was used to wash the samples three times. To fix the cells, 4% paraformaldehyde was added at room temperature. After 30 min, the samples were ready for imaging and the staining was visualized by a Perkin-Elmer Ultraview Vox confocal microscope equipped with a spectral detection system.

3. RESULTS AND DISCUSSION

Uncoated GQDs and PEI-coated GQDs can freely disperse in water and appear light yellow in color. Figure 1 depicts the fluorescence and UV−vis spectra of the diluted solution of the resultant GQDs in aqueous solution. GQDs emit yellow light with a peak at around 550 nm, whereas GQDs with both blue and red light emission could be obtained by coating the GQDs with PEI of different molecular weight (1800 and 600), denoted as PEI_{1800} GQDs and PEI_{600} GQDs, respectively. In aqueous solutions, PEI_{1800} GQDs exhibit blue fluorescence, with λ_{max} at 445 nm and a full width at half-maximum (FWHM) of around 100 nm, and PEI_{600} GQDs show red fluorescence, with a peak at 622 nm and a FWHM of around 100 nm. Figure S3a clearly shows the shift of the PL peak when GQDs were coated with PEI_{600}, and Figure S3b exhibits emission peaks under laser with the same excitation energy at

DOI: 10.1021/acsami.7b05569
ACS Appl. Mater. Interfaces XXXX, XXX, XXX−XXX

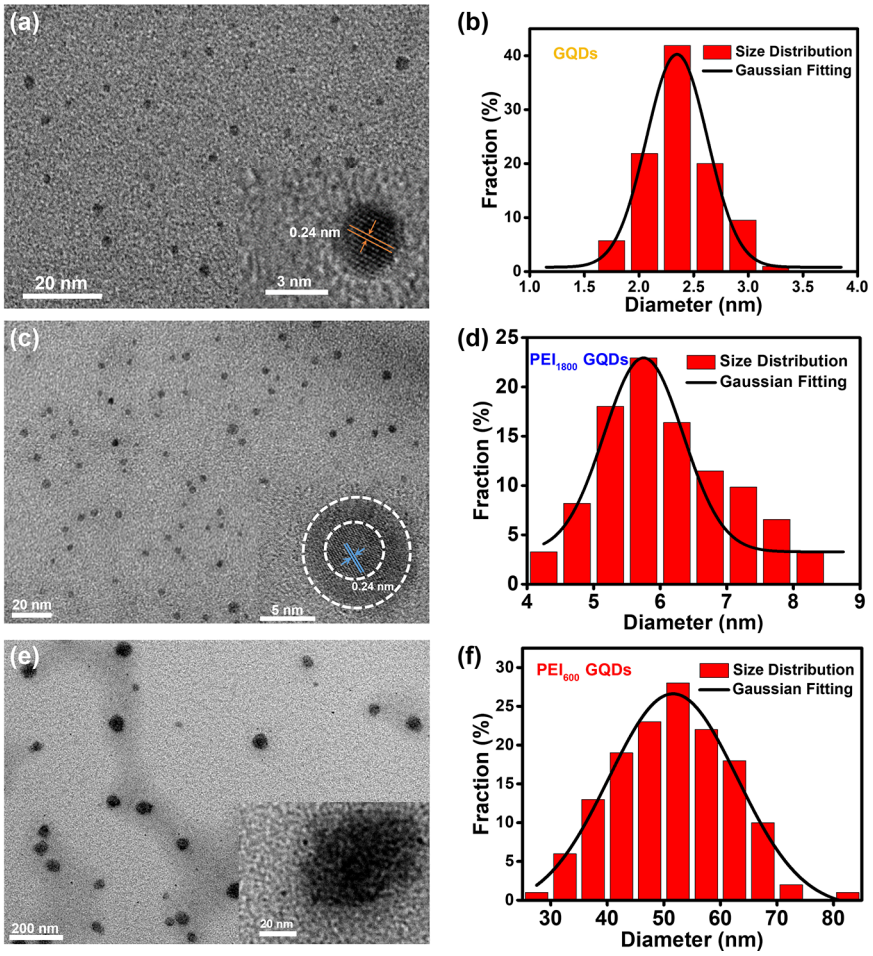

Figure 2. TEM and HRTEM (inset) images of the GQDs (a), PEI_{1800} GQDs (c), and PEI_{600} GQDs (e) assembled on the Cu grid coated with an ultrathin amorphous carbon film. In HRTEM images, both GQDs and the center core of PEI_{1800} GQDs show lattice spacing of about 0.24 nm. (b), (d), and (f): diameter distribution of GQDs, PEI_{1800} GQDs, and PEI_{600} GQDs, respectively. The black line is the Gaussian fitting curve.

365 nm, which indicates that bare GQDs and PEI-coated GQDs can emit light of different colors even under regular UV light. Moreover, the UV−vis spectra also changed (Figure 1d). Bare GQDs and PEI_{600} GQDs showed excitation-dependent PL properties. For instance, the emission maximum shifts from 590 to 690 nm when the excitation wavelength changes from 500 to 650 nm for PEI_{600} GQDs, indicating that PEI_{600} GQDs have different sizes and different emissive sites, which exhibit different PL properties.[40]

HRTEM was used to characterize the morphology, size distribution, and dispersibility information of these GQDs. As shown in Figure 2, taking a numerous amount of samples into account, the average sizes of GQDs, PEI_{1800} GQDs, and PEI_{600} GQDs were determined to be 2.37 ± 0.10 (Figure 2a,b), 6.05 ± 0.77 (Figure 2c,d), and 57.31 ± 8.90 nm (Figure 2e,f), respectively.

Furthermore, the original GQDs have a discernible lattice structure, of which the lattice spacing of GQDs are 0.24 nm (Figure 2a), which is consistent with the d_{1120} lattice plane space of graphene. Interestingly, the HRTEM image of PEI_{1800} GQDs exhibits a core−shell structure, which has a dark black core (the size of the inner core is the same as that of the yellow original GQDs) and a gray outside layer (Figure 2c). Clearly, distinct lattice stripes, with 0.24 nm lattice spacing, corresponding to the graphite d_{1120} lattice plane can be seen in the dark black inner core, but this kind of lattice stripe does not exist in the light gray outside layer, thus indicating a stable core−shell structure formed by coating PEI (gray outside layer) on the surface of bare GQDs (inner dark core). As for PEI_{600} GQDs, relatively huge particles that include multiple GQDs could be observed (Figure 2e).

As shown in Figure 3, the features of these three kinds of GQDs, with a distinct boundary, can be clearly observed from AFM images. The topographic morphology of original GQDs confirms that most GQDs have a thickness below 1 nm (centered at 0.68 nm), which corresponds to the expected thickness of a monolayer or bilayer of GQDs (Figure 3a−c). The AFM image of PEI_{1800} GQDs shows a similar shape and a little larger size compared to those of bare GQDs (Figure 3d). Conversely, from the height profile and distribution, it is easy to find that the average height of PEI_{1800} GQDs is a little larger (Figure 3e,f), which is the result of the coating reaction with PEI_{1800}. Nevertheless, PEI_{600} GQDs are much larger and the average thickness of these GQDs is much greater than that of the former two, which reaches 2.5 nm (Figure 3g−i). All results from the AFM images are in line with those of the TEM images, revealing that the size and thickness of PEI_{600} GQDs are much larger than those of PEI_{1800} GQDs and bare GQDs, whereas PEI_{1800} GQDs are a little bit larger and thicker than uncoated GQDs.

To understand the opposite PL peak shift of the two kinds of PEI-coated GQDs, their different sizes, structures, and

DOI: 10.1021/acsami.7b05569
ACS Appl. Mater. Interfaces XXXX, XXX, XXX−XXX

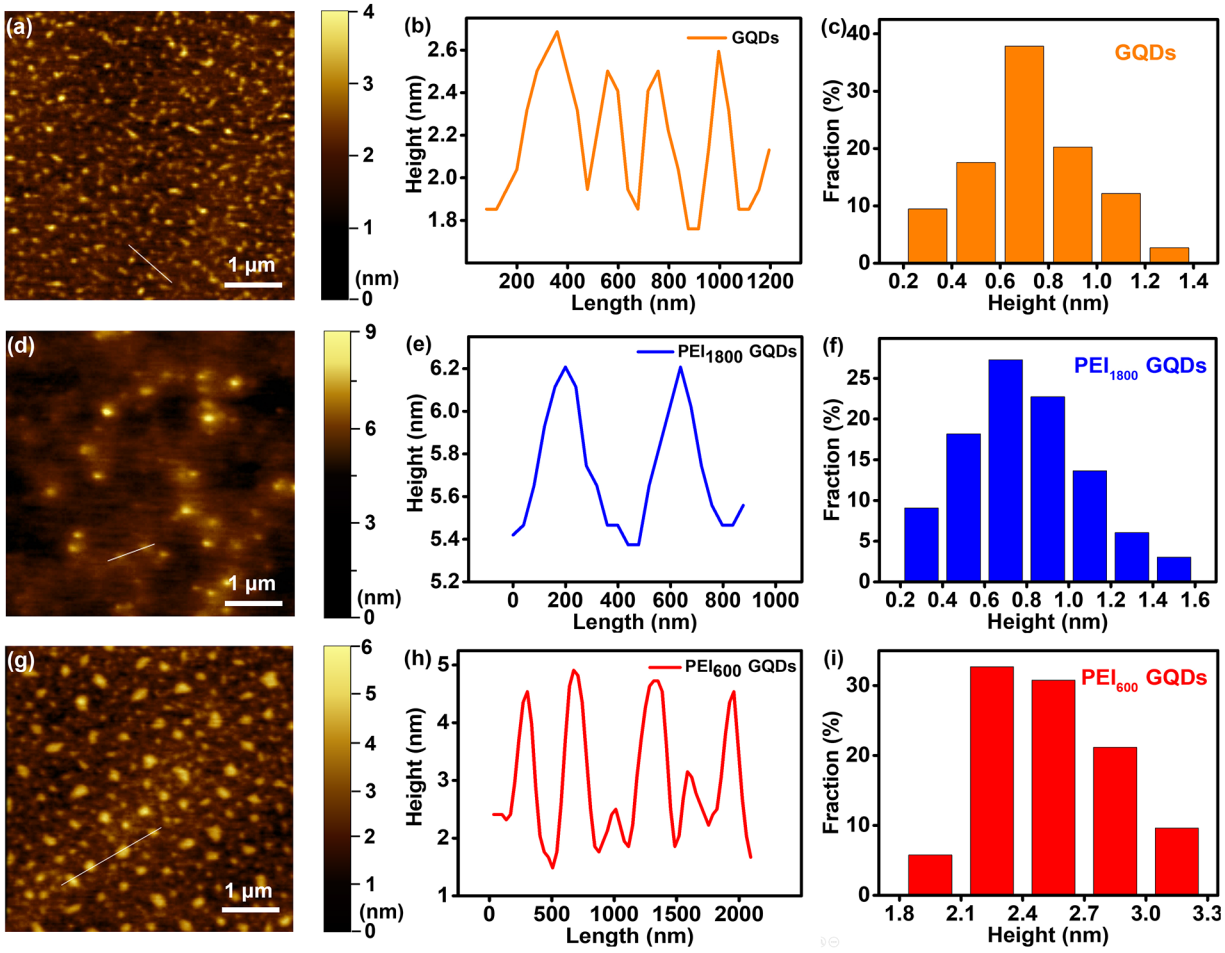

Figure 3. AFM images of the GQDs (a), PEI_{1800} GQDs (d), and PEI_{600} GQDs (g) assembled on mica plate. The side length of each images is 5 μm. GQDs and PEI_{1800} GQDs are monodispersed and show relatively small particle sizes, whereas PEI_{600} GQDs show relatively large particle sizes. (b), (e), and (h): Height profile corresponding to AFM image of GQDs, PEI_{1800} GQDs, and PEI_{600} GQDs, respectively. (c), (f), and (i): Height distribution of GQDs, PEI_{1800} GQDs, and PEI_{600} GQDs, respectively.

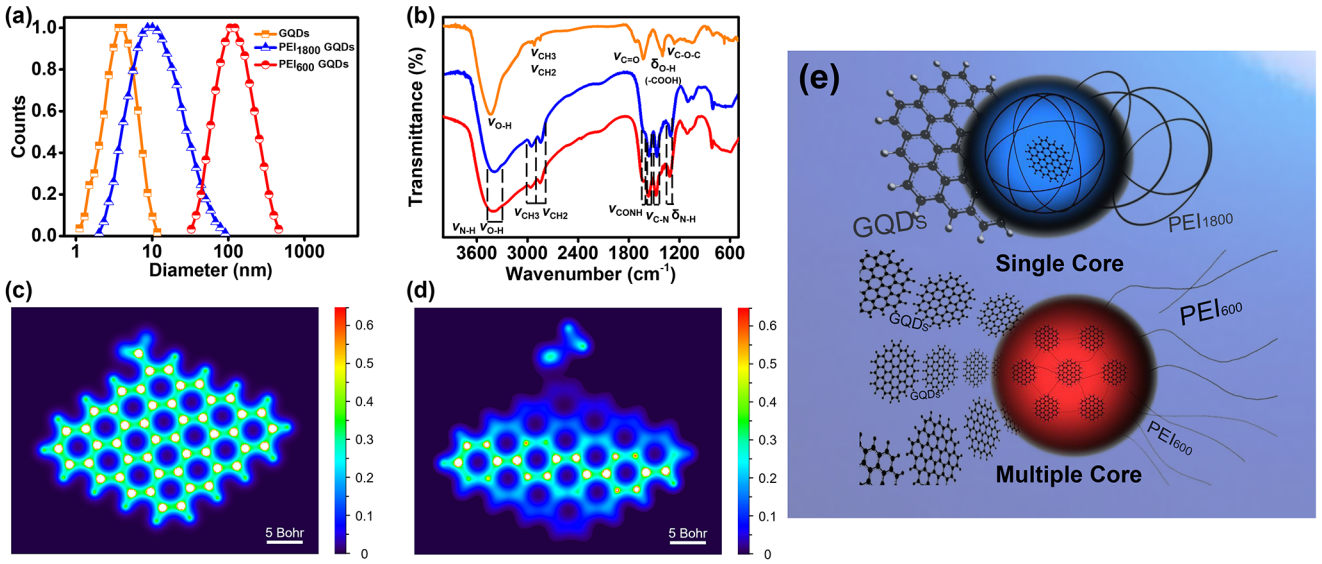

Figure 4. Up: (a) DLS results and (b) FTIR spectra of the GQDs (yellow), PEI_{1800} GQDs (blue), and PEI_{600} GQDs (red). (the color of the lines in the graph are in accord with the emitting light of GQDs). Down: Evidence of the enlargement of the conjugation area after the amidation reaction during the coating process. Charge density graphs of (c) G2 (the only carboxyl group linked with the nanographene core) and (d) G1-N (the nanographene core linked with the PEI branch chain). Right: (e) Scheme of the formation mechanism of blue-emitting PEI_{1800} GQDs (up) and red-emitting PEI_{600} GQDs (down).

DOI: 10.1021/acsami.7b05569
ACS Appl. Mater. Interfaces XXXX, XXX, XXX−XXX

dispersibility were investigated. In the structure of PEI_{1800} GQDs, PEI chains are simply attached onto the GQD by a powerful attraction between the positive charge of PEI and negative charge of GQDs. However, in the case of PEI_{600} GQDs, several GQDs are embedded in the PEI to form a particle that resembles a capsule. The blue shift of PEI_{1800} GQDs can be explained by the conjugation between the amine group of PEI and $\pi-\pi$ domains on the graphene sheet, which lead to an electron transfer and subsequent changes of PL properties. In contrast, the red shift of the PL of PEI_{600} GQDs indicates that the conjugated system is enlarged by the connection of a few GQDs, in which the cross-linking of PEI_{600} plays an important role. In other words, the red-shifted PL is derived from the cross-linking enhanced emission effect. Specifically, with PEI-coated multiple graphene cores, the vibration and rotation of the cross-linking PEI-GQD system is reduced and the effective emission region is extended; thus, an enhanced red-shifted PL can be observed.[41]

In corroboration to these findings, DLS was utilized to study the size distribution of PEI-coated GQDs. As shown in Figure 4a, the average particle diameters of GQDs, PEI_{1800} GQDs, and PEI_{600} GQDs are 3.9, 9.5, and 112.1 nm, respectively. Thus, the distribution trend perfectly agrees with the TEM characterization.

Furthermore, FTIR spectroscopy and XRD were adopted to prove that the GQDs had been completely coated by PEI. FTIR spectra of PEI_{1800} GQDs and PEI_{600} GQDs show a striking similarity, even though the spectra of GQDs are quite different (Figure 4b). For original GQDs, the characteristic absorption peak at around 3450 cm^{-1} is assigned to the stretching vibration of −OH. The peaks at 2919 and 2839 cm^{-1} are ascribed to stretching vibrations of −CH. The typical peaks at 1725 and 1400 cm^{-1} are associated with the stretching vibration of C═O and bending vibrations of −OH (in −COOH), respectively. The peak at 1629 cm^{-1} can be ascribed to aromatic stretching vibration of graphite domains, and the peak at 1260 cm^{-1} is related to the stretching vibration of C−O−C.[42] For the two PEI-coated GQDs, the absorption peaks at around 3386 cm^{-1} are assigned to the stretching vibrations of $-NH_2$ and −OH.[43] The peaks at 2955 and 2846 cm^{-1} are ascribed to the stretching vibrations of −CH. The typical peaks at 1570 and 1650 cm^{-1} are associated with bending vibrations of −CONH−. The peak at 1479 cm^{-1} is related to the stretching of C−N, and the peak at 1315 cm^{-1} is ascribed to the bending vibration of N−H.[1,44] The results above indicate that compared with the original GQDs, PEI-coated GQDs own new functional groups, such as $-NH_2$, −CONH−, and C−N functional groups, along with an absence of the −COOH functional group. Therefore, it can be inferred from the changes that the amine groups in PEI have reacted with the carboxyl groups on the surface of GQDs to form amide bonds. Further, in terms of the vanishing of carboxyl groups in PEI-coated GQDs, it can be deduced that PEI chains have completely coated GQDs by the amidation reaction. Identical conclusions were obtained in analyzing XPS and high-resolution XPS spectra (HRXPS) results (Figure S4) and elemental contents from XPS (Table S1) of bare GQDs and PEI-coated GQDs. On one hand, from survey XPS spectra, it is observed that nitrogen peaks appear in spectra of PEI-coated GQDs; however, there is no obvious nitrogen peak in those of bare GQDs. After further investigation of their C 1s and N 1s HRXPS spectra, it shows that only bare GQDs have the −COOH peak at 288.5 eV and only PEI-coated GQDs have −CN and −C═O peaks for amide functional groups (−CONHR) at 285.8 and 287.6 eV, respectively. In addition, only PEI-coated GQDs possess $-NH_2$ peaks and −CONHR peaks in N 1s HRXPS spectra. On the other hand, as shown in Table S1, elemental contents of GQDs and PEI-coated GQDs from XPS revealed that the (N 1s)/(C 1s) atomic ratio increased and the (O 1s)/(C 1s) atomic ratio decreased after GQDs being coated with PEI, which illustrated the amidation reaction process which added nitrogen atoms and lost oxygen atoms at the same time. Thus, this further proved that carboxyl functional groups were changed to amide functional groups during the coating reaction. Figure S5 presents XRD patterns of GQDs, PEI_{1800} GQDs, and PEI_{600} GQD powders. Like the FTIR spectra above, XRD patterns of PEI_{1800} GQDs, and PEI_{600} GQDs are very similar. The weak, broad (002) peak in XRD patterns located at around 23.1° indicates the thinness and stacking structure of graphene layers.[45] However, the peak moved to 20°, which means the lattice parameter increased, when PEI was coated on the surface of bare GQDs to form PEI_{1800} GQDs and PEI_{600} GQDs particles. This peak movement indicated that a stable thicker core−shell structure with disordered atoms from the PEI chain was formed after the coating reactions.

To explore the detailed mechanism of the combination of GQDs and PEI, zeta potentials of GQDs, PEI_{1800} GQDs, and PEI_{600} GQDs were determined at pH 7 in aqueous solution (Figure S6). The surface of GQDs is mainly negatively charged with a zeta potential of −57.27 mV. It is well known that the higher the absolute value of the zeta potential is, the better the dispersion will be.[46] However, when the GQDs are coated with PEI, zeta potentials of stable PEI_{1800} GQDs and PEI_{600} GQDs are −0.27 and −3.27 mV, respectively. Their resulting stability is beneficial to applications in complex environments.[47] In summary, the formation of PEI-coated GQDs was caused by the amidation reaction. However, this may also partly result from electrostatic interactions between GQDs and PEI because the latter polymer is a well-known electron acceptor, whereas GQDs are electron donors.

Figure 4e shows a representation of the formation process of two PEI-coated GQDs. PEI of different molecular weights interact with GQDs in different ways. When PEI_{1800} of a larger size connects with a GQD to form a particle, it cannot connect with another particle. Thus, PEI of high molecular weight forms single core structures, which resembles jellybeans. PEI_{600} is much shorter than PEI_{1800}. Correspondingly, the reaction activity is much stronger than that of PEI_{1800}, so multiple-core structures can be formed by using PEI_{600} because many PEI_{600} beads can connect to form a big PEI cage, which can contain several GQDs. These structures are similar to a capsule because the PEI cage is like a big soft shell and GQDs are like particles inside the capsule shell.

Our data provides an explanation on how the structures of the three kinds of GQDs cause changes in PL properties of PEI-GQDs during the process of the coating reaction. In previous studies, conventional coating reactions by polymers could affect the PL intensity of GQDs, which was quite useful in a variety of fields, but the strategies did not substantially change the emission maxima of GQDs.[35,48−51] However, in our work, we can realize both a large blue shift and a large red shift of the emission maxima of GQDs by using only one kind of polymer. As a result, blue-, yellow-, and red-emitting GQDs can be obtained, which illustrates a method for developing tunable PL GQDs. For PEI_{1800} GQDs, the single layer PEI-coated

DOI: 10.1021/acsami.7b05569
ACS Appl. Mater. Interfaces XXXX, XXX, XXX−XXX

core−shell structure contributes to the blue shift of the PL peaks. On the contrary, the most critical factor of the red shift of PEI_{600} GQDs is the interaction of multiple GQD particles in a larger PEI cage.

The PL mechanism of GQDs is complicated and various factors can affect PL properties of GQDs. In addition to the quantum confinement effect, which is the key factor in conventional semiconductor quantum dots, other factors, like size, elemental composition, surface functional groups, edge states, and defects in the carbon bone structure can affect PL properties.[52−54] Previously, researchers put forth that the PL mechanism can be explained by examining the surface/edge state and conjugated π-domains. Because the emission maximum of PEI_{1800} GQDs exhibits a distinct blue shift, it can be deduced that the graphene core maintains its own character even though the surface state changes a lot. The most significant change is that the carboxyl groups on the surface of GQDs have reacted with amine groups of PEI to form amide bonds, which lead to the linkage of GQDs and PEI_{1800}. It was found that both the molecule-like defect state and intrinsic state existed in GQDs. Always, the molecule-like defect state stems from carboxyl groups, whereas the core structure makes for the intrinsic state. During the coating treatment, −COOH reacted with the amine group to form −CONHR, which transfered GQDs from defect state emission into intrinsic state emission. Therefore, the peak at 520 nm corresponding to the defect state disappeared and at the same time the peak at 435 nm, which was attributed to the intrinsic state, appeared after the coating process. The conjugation mode between the carboxyl group and the inner graphene core is $\pi-\pi$ and $p-\pi$ mode, with all atoms on the same plane except for the H atom on the tail end of the carboxyl group (Figure S7). Thus, the functional groups play a leading role, because the defect state caused by the carboxyl group determines the band gap, whereas in the structure of −CONHR, all atoms in −CONHC− and the inner graphene core are on the same plane and the electron cloud of lone pair electrons in N is overlapped with that of −C═O, forming a strong $p-\pi$ conjugation. Therefore, the interaction between the amide bond and the graphene core is quite weak. As a result, the amidation reaction transferred GQDs from defect state emission to intrinsic state emission. As a result, the PL peak was blue-shifted from 510 to 435 nm and the emission color was changed from yellow to blue (Figure 1b).

In red-emitting PEI-coated GQDs, the interaction between GQD particles in the big capsule plays a vital role in red-shifted emission. As reported, PL properties of GQDs can be tuned by the size of conjugated π-domains. Typically, as the particles get bigger, luminescence energies move toward lower energy. In PEI_{600} GQDs, some GQDs were constrained in a small cage formed by PEI, so the GQDs are close to each other, arranged parallelly or stacked. Thus, when the distance between the GQDs is close enough, electrons can move freely between different GQDs. Thus, the conjugated π-domains are enlarged, and the energy band gap of PEI_{600} GQDs is narrowed compared to that of monodispersed uncoated GQDs. This causes a red shift in the PL emission.[55]

Because it is quite difficult to study a single nanoparticle by traditional methods, theoretical calculations were used to understand the PL mechanism.[18] As shown in Figure S8, the conjugation mode between the two functional groups and inner graphene core was calculated. By theoretical calculation with DFT B3LYP/6-31G*, molecular orbitals of amide-GQD G1 ($C_{50}H_{21}NO$) (Figure S8a), carboxyl-GQD G2 ($C_{49}H_{18}O_2$) (Figure S8b), and G1-N ($C_{53}H_{28}N_2O$) (Figure S8c) were obtained.[56,57] G1 and G2 are different in the linking groups and G1-N simulates a real PEI branch chain. The highest occupied molecular orbital and lowest unoccupied molecular orbital play important roles in the chemical and PL properties of a compound.[58] Compared with carboxyl-GQDs, amide-GQDs can induce a bigger energy gap. Although there are always many functional groups linked to the graphene core, in the theoretical calculation, only one functional group was taken into account for convenience. Therefore, the influence caused by amidation of carboxyl groups may be much more significant in the real system. As a result, the changes of the energy gap of PEI-GQDs would be influenced cumulatively. When the band gap is enlarged, the PL emission peak will be blue-shifted, because the width of the band gap is positively correlated with that of the energy gap.[59,60]

Other models of nanographene cores with acetamide, butyrylamide, and a part of the PEI chain were calculated to study the effect of alkyl chain length and simulate the real PEI-coated GQD system (Figure S8d). Energy gaps of G1, G1-N, G1-2C ($C_{51}H_{23}NO$), G1-3C ($C_{52}H_{25}NO$), G1-4C ($C_{53}H_{27}NO$), and G1-5C ($C_{54}H_{29}NO$) do not change with the increasing length of the carbon chain (Figure S8d and Table S2). Additionally, the branch chains in PEI do not affect the orbitals. These calculations suggest good reliability of theoretical simulation with the key linking group (−CONH−) instead of the whole PEI molecule.

Moreover, the electron density is also a key factor of PL properties. The carboxyl group shares the charge completely with the inner graphene core (Figure 4c). In the charge density of G1-N that is formed by an amidation reaction between GQDs and PEI, electrons are concentrated on the center of the inner core when the PEI end chain is linked to the core (Figure 4d). The conjugation structure is closely related to electron distribution, so the conjugation domain was narrowed when PEI was coated on the graphene core. As it is well known, when the conjugation domain is reduced, the band gap will always be enlarged. Therefore, when PEI_{1800} GQDs were generated, it would emit light with more energy. Thereby, the PL maximum of light emitting materials would be blue-shifted and thus the charge density distribution agreed with the theoretical calculations. It also gave a strong support to demonstrate the state changing process mentioned above; namely, after coating with PEI_{1800}, the influence of the "defect state" caused by functional groups was sharply reduced and the "intrinsic state" from the inner graphene core, which always gave a blue light emission, played a vital role in the PL generation process. Moreover, for GQDs which are around 15 aromatic rings, especially for the regular inner core in blue-emitting GQDs, the band gaps of size/edge-related intrinsic states are similar.[61] However, the yellow-emitting bare GQDs have various emission sites aroused by different kinds of defect states from functional groups on different positions of GQDs. Hence, the blue-emitting PEI_{1800} GQDs show an excitation-independent emission property, which is different with bare GQDs and red-emitting PEI_{600} GQDs.

To further understand how coatings affect the PL mechanism, the fluorescent lifetimes of GQDs were measured by time-resolved fluorescence spectroscopy (Figure S9a). Fluorescence lifetimes of bare GQDs, blue-emitting PEI_{1800} GQDs, and red-emitting PEI_{600} GQDs are 2.19, 5.53, and 3.32 ns, respectively. Thus, fluorescence lifetimes are changed after coating with PEI and different PEI coatings result in different

DOI: 10.1021/acsami.7b05569
ACS Appl. Mater. Interfaces XXXX, XXX, XXX−XXX

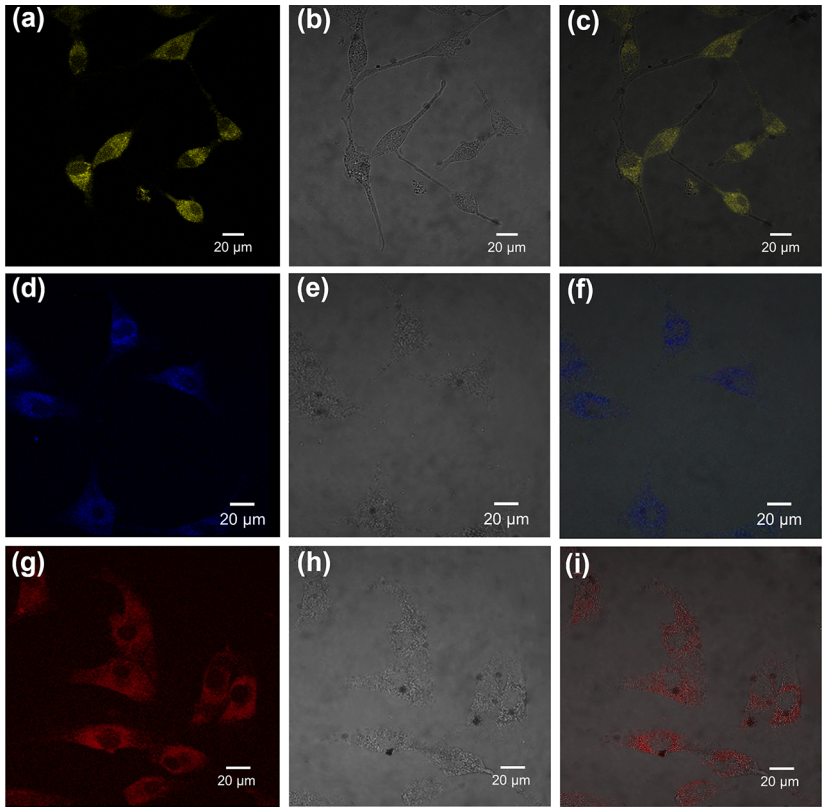

Figure 5. Confocal fluorescence images of U-87 cells incubated with 50 μg mL^{-1} GQDs (a–c), PEI_{1800} GQDs (d–f), and PEI_{600} GQDs (g–i) for 18 h. (a), (d), and (g) are the fluorescence images of U-87 cells labeled with these three GQDs, with excitation at 405 nm. (b), (e), and (h) are the bright-field images of U-87 cells. (c), (f), and (i) are the merged images of U-87 cells incubated with three GQDs.

lifetimes. These results imply that changes in PL properties of the coated GQDs are caused by the reaction between PEI and GQDs, rather than the inner-filter effect of fluorescence.[62,63] Therefore, taking all of these data above into account, it can be inferred that the coating reaction mechanism was a synergy of the amidation reaction and electrostatic interaction of GQDs with PEI.

In addition, stability of these three GQDs under various conditions has been investigated. When applied as probes or sensors,[64] fluorescent nanomaterials always need to be repeatedly excited, so high stability under repeated excitation with lasers is quite necessary. PL intensities of these three GQDs remain constant for the first 100 excitations at their excitation maxima (Figure S9b). Furthermore, there is no change in PL intensity for these GQDs at different concentrations of KCl (Figure S9c), which indicates that PL properties will not be affected by varying ionic strength. This robustness makes these GQDs useful for practical applications that involve the presence of high salt concentrations. As illustrated in Figure S9d, these GQDs exhibit excellent PL stability under irradiation with a UV lamp (24 W) at 365 nm, showing an antiphotobleaching property, which is necessary for long time exposure in real applications, such as labeling and tracing.

Biocompatibility of nanomaterials is quite important for biomedical applications.[65−68] The stability of these GQDs in physiological conditions was tested. After incubation in a DMEM culture supplemented with 10% FBS, saline, or only FBS for 72 h, these three GQDs did not form any floccules or sediment, which demonstrated that GQDs were stable in the physiological condition. The cell viability of human embryonic kidney cell line 293 (HEK-293) and human primary glioblastoma cell line 87 (U-87) cells was examined when exposed to 0−200 μg mL^{-1} of PEI_{1800} GQDs, GQDs, and PEI_{600} GQDs for 24 h (Figure S10). There was no substantial reduction of cell viability for both cell lines when exposed to high concentrations (up to 200 μg mL^{-1}) of GQDs. In general, these three GQDs are of quite low cytotoxicity, indicating that the as-prepared GQDs with favorable biocompatibility have good potential to be used in bioimaging, biosensing, and so forth.

Moreover, GQDs were developed as bioimaging agents. In detail, U-87 cells were incubated with uncoated GQDs, PEI_{1800} GQDs, and PEI_{600} GQDs for 18 h, respectively, and subsequently were observed by confocal laser scanning microscopy (Figure 5a,d,g). U-87 cells exhibit bright yellow, bright blue, and bright red PL when excited with 405 nm light after incubation with uncoated GQDs, PEI_{1800} GQDs, and PEI_{600} GQDs, respectively. From bright field images of U-87 cells (Figure 5b,e,h), the morphology of cells further verifies that these three GQDs possess quite low cytotoxicity. Merged images (Figure 5c,f,i) further prove the capability of the as-prepared GQDs to penetrate into cells without any further treatment. These results demonstrate that the GQDs in this work are very promising for bioimaging of different kinds of living cells.

4. CONCLUSIONS

In summary, PL-tunable GQDs with blue, yellow, and red emission colors were synthesized by coating with PEI of different molecular weights. TEM, AFM, XRD, FTIR, XPS, DLS, and zeta potential were employed to characterize the

DOI: 10.1021/acsami.7b05569
ACS Appl. Mater. Interfaces XXXX, XXX, XXX−XXX

structures of the as-prepared GQDs. The PL mechanism was studied by theoretical calculations. The average sizes of uncoated yellow-emitting GQDs, blue-emitting PEI_{1800} GQDs, and red-emitting PEI_{600} GQDs were 2.37, 6.05, and 57.31 nm, respectively. The yellow-emitting and blue-emitting GQDs were monolayer structures, whereas the red-emitting GQDs were multilayer structures. The red-emitting GQDs possessed a big PEI cage with multiple GQDs inside, whereas the blue-emitting PEI-coated GQDs had a single GQD core. Carboxyl groups were changed to amide groups on the surface of GQDs, so the influence of those functional groups was studied using theoretical calculation with DFT B3LYP/6-31G*. The amidation reaction was crucial for PL change. By analyzing the molecular orbital and charge density, it was found that amide bonds decreased the conjugation and increased the energy gap thus inducing the blue shift of the PL. For the red-emitting GQDs, the conjugation area was enlarged by the interaction of GQDs in the PEI cage; thus, the PL peak exhibited a red shift. Remarkably, all GQDs exhibited good stability at high ionic strength and resisted photobleaching. Cell viability after treatment with the as-prepared GQDs indicated that GQDs had quite low cytotoxicity. Finally, the GQDs could be used for bioimaging and are expected to be widely applied in multicolor imaging and bioanalysis applications. We hope that this work will inspire the design of even better GQDs with tunable PL properties.

■ ASSOCIATED CONTENT

Supporting Information

The Supporting Information is available free of charge on the ACS Publications website at DOI: 10.1021/acsami.7b05569.

Syntheses process (Figure S1); photos of GQDs powder (Figure S2); excitation-dependent PL spectra and PL spectra under UV lamp (Figure S3); XPS and HRXPS (Figure S4), elemental content analyses (Table S1), XRD spectra (Figure S5), zeta potential (Figure S6) of GQDS; schematic diagram of the key reaction (Figure S7); theoretical calculation results (Figure S8), energy gap information (Table S2), PL lifetime and chemical and optical stability of GQDs (Figure S9); biological stability and the toxicity test of GQDs (Figure S10); QY measurements of GQDs (Figure S11 and Table S3) (PDF)

■ AUTHOR INFORMATION

Corresponding Authors

*Email: fljiang@whu.edu.cn. Tel: +86-27-68756667 (F.L.J.).
*E-mail: yiliuchem@whu.edu.cn. Tel: +86-27-68753465 (Y.L.).

ORCID

Tian Gao: 0000-0003-0304-3228
Feng-Lei Jiang: 0000-0002-1008-6042
Yi Liu: 0000-0001-7626-0026

Notes

The authors declare no competing financial interest.

■ ACKNOWLEDGMENTS

The authors gratefully acknowledge the financial support from National Natural Science Foundation of China (21473125, 21573168), National Science Fund for Distinguished Young Scholars of China (21225313), Bagui Scholar Program of Guangxi Province, Natural Science Foundation of Hubei Province (2014CFA003), and Large-scale Instrument and Equipment Sharing Foundation of Wuhan University.

■ REFERENCES

(1) Moon, B. J.; Lee, K. S.; Shim, J.; Park, S.; Kim, S. H.; Bae, S.; Park, M.; Lee, C.-L.; Choi, W. K.; Yi, Y.; Hwang, J. Y.; Son, D. I. Enhanced Photovoltaic Performance of Inverted Polymer Solar Cells Utilizing Versatile Chemically Functionalized Zno@Graphene Quantum Dot Monolayer. *Nano Energy* **2016**, *20*, 221−232.

(2) Yang, H. B.; Dong, Y. Q.; Wang, X.; Khoo, S. Y.; Liu, B. Cesium Carbonate Functionalized Graphene Quantum Dots as Stable Electron-Selective Layer for Improvement of Inverted Polymer Solar Cells. *ACS Appl. Mater. Interfaces* **2014**, *6*, 1092−1099.

(3) Li, N.; Than, A.; Wang, X.; Xu, S.; Sun, L.; Duan, H.; Xu, C.; Chen, P. Ultrasensitive Profiling of Metabolites Using Tyramine-Functionalized Graphene Quantum Dots. *ACS Nano* **2016**, *10*, 3622−3629.

(4) Liu, Q.; Guo, B.; Rao, Z.; Zhang, B.; Gong, J. R. Strong Two-Photon-Induced Fluorescence from Photostable, Biocompatible Nitrogen-Doped Graphene Quantum Dots for Cellular and Deep-Tissue Imaging. *Nano Lett.* **2013**, *13*, 2436−2441.

(5) Chong, Y.; Ma, Y.; Shen, H.; Tu, X.; Zhou, X.; Xu, J.; Dai, J.; Fan, S.; Zhang, Z. The in Vitro and in Vivo Toxicity of Graphene Quantum Dots. *Biomaterials* **2014**, *35*, 5041−5048.

(6) Ge, J.; Lan, M.; Zhou, B.; Liu, W.; Guo, L.; Wang, H.; Jia, Q.; Niu, G.; Huang, X.; Zhou, H.; Meng, X.; Wang, P.; Lee, C. S.; Zhang, W.; Han, X. A Graphene Quantum Dot Photodynamic Therapy Agent with High Singlet Oxygen Generation. *Nat. Commun.* **2014**, *5*, No. 4596.

(7) Ghafouri, R. Exploring Pentagon-Heptagon Pair Defects in the Triangular Graphene Quantum Dots: A Computational Study. *Mater. Chem. Phys.* **2016**, *175*, 223−232.

(8) Sudhagar, P.; Herraiz-Cardona, I.; Park, H.; Song, T.; Noh, S. H.; Gimenez, S.; Sero, I. M.; Fabregat-Santiago, F.; Bisquert, J.; Terashima, C.; Paik, U.; Kang, Y. S.; Fujishima, A.; Han, T. H. Exploring Graphene Quantum Dots/Tio2 Interface in Photoelectrochemical Reactions: Solar to Fuel Conversion. *Electrochim. Acta* **2016**, *187*, 249−255.

(9) Liu, F.; Jang, M. H.; Ha, H. D.; Kim, J. H.; Cho, Y. H.; Seo, T. S. Facile Synthetic Method for Pristine Graphene Quantum Dots and Graphene Oxide Quantum Dots: Origin of Blue and Green Luminescence. *Adv. Mater.* **2013**, *25*, 3657−3662.

(10) Tetsuka, H.; Asahi, R.; Nagoya, A.; Okamoto, K.; Tajima, I.; Ohta, R.; Okamoto, A. Optically Tunable Amino-Functionalized Graphene Quantum Dots. *Adv. Mater.* **2012**, *24*, 5333−5338.

(11) Ananthanarayanan, A.; Wang, X.; Routh, P.; Sana, B.; Lim, S.; Kim, D.-H.; Lim, K.-H.; Li, J.; Chen, P. Facile Synthesis of Graphene Quantum Dots from 3d Graphene and Their Application for Fe3+Sensing. *Adv. Funct. Mater.* **2014**, *24*, 3021−3026.

(12) Peng, J.; Gao, W.; Gupta, B. K.; Liu, Z.; Romero-Aburto, R.; Ge, L.; Song, L.; Alemany, L. B.; Zhan, X.; Gao, G.; Vithayathil, S. A.; Kaipparettu, B. A.; Marti, A. A.; Hayashi, T.; Zhu, J. J.; Ajayan, P. M. Graphene Quantum Dots Derived from Carbon Fibers. *Nano Lett.* **2012**, *12*, 844−849.

(13) Liu, R.; Wu, D.; Feng, X.; Mullen, K. Bottom-up Fabrication of Photoluminescent Graphene Quantum Dots with Uniform Morphology. *J. Am. Chem. Soc.* **2011**, *133*, 15221−15223.

(14) Zhu, S.; Song, Y.; Zhao, X.; Shao, J.; Zhang, J.; Yang, B. The Photoluminescence Mechanism in Carbon Dots (Graphene Quantum Dots, Carbon Nanodots, and Polymer Dots): Current State and Future Perspective. *Nano Res.* **2015**, *8*, 355−381.

(15) Zhu, S.; Zhang, J.; Qiao, C.; Tang, S.; Li, Y.; Yuan, W.; Li, B.; Tian, L.; Liu, F.; Hu, R.; Gao, H.; Wei, H.; Zhang, H.; Sun, H.; Yang, B. Strongly Green-Photoluminescent Graphene Quantum Dots for Bioimaging Applications. *Chem. Commun.* **2011**, *47*, 6858−6860.

(16) Dong, Y.; Chen, C.; Zheng, X.; Gao, L.; Cui, Z.; Yang, H.; Guo, C.; Chi, Y.; Li, C. M. One-Step and High Yield Simultaneous Preparation of Single- and Multi-Layer Graphene Quantum Dots from Cx-72 Carbon Black. *J. Mater. Chem.* **2012**, *22*, 8764−8766.

DOI: 10.1021/acsami.7b05569
ACS Appl. Mater. Interfaces XXXX, XXX, XXX−XXX

(17) Jiang, K.; Sun, S.; Zhang, L.; Lu, Y.; Wu, A.; Cai, C.; Lin, H. Red, Green, and Blue Luminescence by Carbon Dots: Full-Color Emission Tuning and Multicolor Cellular Imaging. *Angew. Chem., Int. Ed. Engl.* **2015**, *54*, 5360−5363.
(18) Xu, Z. Q.; Lan, J. Y.; Jin, J. C.; Gao, T.; Pan, L. L.; Jiang, F. L.; Liu, Y. Mechanistic Studies on the Reversible Photophysical Properties of Carbon Nanodots at Different Ph. *Colloids Surf., B* **2015**, *130*, 207−214.
(19) Hu, S.; Trinchi, A.; Atkin, P.; Cole, I. Tunable Photoluminescence across the Entire Visible Spectrum from Carbon Dots Excited by White Light. *Angew. Chem., Int. Ed. Engl.* **2015**, *54*, 2970−2974.
(20) Ke, C.-C.; Yang, Y.-C.; Tseng, W.-L. Synthesis of Blue-, Green-, Yellow-, and Red-Emitting Graphene-Quantum-Dot-Based Nanomaterials with Excitation-Independent Emission. *Part. Part. Syst. Charact.* **2016**, *33*, 132−139.
(21) Sapkota, B.; Benabbas, A.; Lin, H. G.; Liang, W.; Champion, P.; Wanunu, M. Peptide-Decorated Tunable-Fluorescence Graphene Quantum Dots. *ACS Appl. Mater. Interfaces* **2017**, *9*, 9378−9387.
(22) Zhu, S.; Wang, L.; Li, B.; Song, Y.; Zhao, X.; Zhang, G.; Zhang, S.; Lu, S.; Zhang, J.; Wang, H.; Sun, H.; Yang, B. Investigation of Photoluminescence Mechanism of Graphene Quantum Dots and Evaluation of Their Assembly into Polymer Dots. *Carbon* **2014**, *77*, 462−472.
(23) Hu, Y.; He, D.-W.; Wang, Y.-S.; Duan, J.-H.; Wang, S.-F.; Fu, M.; Wang, W.-S. An Approach to Controlling the Fluorescence of Graphene Quantum Dots: From Surface Oxidation to Fluorescent Mechanism. *Chin. Phys. B* **2014**, *23*, No. 128103.
(24) Zhu, S.; Zhang, J.; Tang, S.; Qiao, C.; Wang, L.; Wang, H.; Liu, X.; Li, B.; Li, Y.; Yu, W.; Wang, X.; Sun, H.; Yang, B. Surface Chemistry Routes to Modulate the Photoluminescence of Graphene Quantum Dots: From Fluorescence Mechanism to up-Conversion Bioimaging Applications. *Adv. Funct. Mater.* **2012**, *22*, 4732−4740.
(25) Zhang, X.-P.; Hou, Y.-H.; Wang, L.; Zhang, Y.-Z.; Liu, Y. Exploring the Mechanism of Interaction between Sulindac and Human Serum Albumin: Spectroscopic and Molecular Modeling Methods. *J. Lumin.* **2013**, *138*, 8−14.
(26) Sheng, W.-d.; Korkusinski, M.; Güçlü, A. D.; Zielinski, M.; Potasz, P.; Kadantsev, E. S.; Voznyy, O.; Hawrylak, P. Electronic and Optical Properties of Semiconductor and Graphene Quantum Dots. *Front. Phys.* **2011**, *7*, 328−352.
(27) Zhao, J.; Tang, L.; Xiang, J.; Ji, R.; Hu, Y.; Yuan, J.; Zhao, J.; Tai, Y.; Cai, Y. Fabrication and Properties of a High-Performance Chlorine Doped Graphene Quantum Dot Based Photovoltaic Detector. *RSC Adv.* **2015**, *5*, 29222−29229.
(28) Chen, H.; Li, W.; Zhao, P.; Nie, Z.; Yao, S. A Cdte/Cds Quantum Dots Amplified Graphene Quantum Dots Anodic Electrochemiluminescence Platform and the Application for Ascorbic Acid Detection in Fruits. *Electrochim. Acta* **2015**, *178*, 407−413.
(29) Dong, Y.; Pang, H.; Yang, H. B.; Guo, C.; Shao, J.; Chi, Y.; Li, C. M.; Yu, T. Carbon-Based Dots Co-Doped with Nitrogen and Sulfur for High Quantum Yield and Excitation-Independent Emission. *Angew. Chem., Int. Ed. Engl.* **2013**, *52*, 7800−7804.
(30) Zhu, S.; Tang, S.; Zhang, J.; Yang, B. Control the Size and Surface Chemistry of Graphene for the Rising Fluorescent Materials. *Chem. Commun.* **2012**, *48*, 4527−4539.
(31) Chandra, S.; Patra, P.; Pathan, S. H.; Roy, S.; Mitra, S.; Layek, A.; Bhar, R.; Pramanik, P.; Goswami, A. Luminescent S-Doped Carbon Dots: An Emergent Architecture for Multimodal Applications. *J. Mater. Chem. B* **2013**, *1*, 2375−2382.
(32) Lingam, K.; Podila, R.; Qian, H.; Serkiz, S.; Rao, A. M. Evidence for Edge-State Photoluminescence in Graphene Quantum Dots. *Adv. Funct. Mater.* **2013**, *23*, 5062−5065.
(33) Nurunnabi, M.; Khatun, Z.; Nafiujjaman, M.; Lee, D. G.; Lee, Y. K. Surface Coating of Graphene Quantum Dots Using Mussel-Inspired Polydopamine for Biomedical Optical Imaging. *ACS Appl. Mater. Interfaces* **2013**, *5*, 8246−8253.
(34) Gonçalves, H. M.; Duarte, A. J.; Davis, F.; Higson, S. P.; Esteves da Silva, J. C. Layer-by-Layer Immobilization of Carbon Dots Fluorescent Nanomaterials on Single Optical Fiber. *Anal. Chim. Acta* **2012**, *735*, 90−95.
(35) Ding, H.; Zhang, P.; Wang, T. Y.; Kong, J. L.; Xiong, H. M. Nitrogen-Doped Carbon Dots Derived from Polyvinyl Pyrrolidone and Their Multicolor Cell Imaging. *Nanotechnology* **2014**, *25*, No. 205604.
(36) Shen, J.; Zhu, Y.; Yang, X.; Zong, J.; Zhang, J.; Li, C. One-Pot Hydrothermal Synthesis of Graphenequantum Dots Surface-Passivated by Polyethylene Glycol and Their Photoelectric Conversion under near-Infrared Light. *New J. Chem.* **2012**, *36*, 97−101.
(37) Ogris, M.; Brunner, S.; Schüller, S.; Kircheis, R.; Wagner, E. Pegylated DNA/Transferrin-Pei Complexes: Reduced Interaction with Blood Components, Extended Circulation in Blood and Potential for Systemic Gene Delivery. *Gene Ther.* **1999**, *6*, 595−605.
(38) Zhao, H.-X.; Wang, Y.-C.; Zhang, L.-Y.; Wang, M. One- and Two-Photon Luminescence in Graphene Oxide Quantum Dots. *New J. Chem.* **2015**, *39*, 98−101.
(39) Parr, R. G.; Yang, W. *Density-Functional Theory of Atoms and Molecules*; Oxford University Press: New York, 1989.
(40) Saidi, W. A. Oxygen Reduction Electrocatalysis Using N-Doped Graphene Quantum-Dots. *J. Phys. Chem. Lett.* **2013**, *4*, 4160−4165.
(41) Zhu, S.; Wang, L.; Zhou, N.; Zhao, X.; Song, Y.; Maharjan, S.; Zhang, J.; Lu, L.; Wang, H.; Yang, B. The Crosslink Enhanced Emission (Cee) in Non-Conjugated Polymer Dots: From the Photoluminescence Mechanism to the Cellular Uptake Mechanism and Internalization. *Chem. Commun.* **2014**, *50*, 13845−13848.
(42) Hu, L.; Li, D.-B.; Gao, L.; Tan, H.; Chen, C.; Li, K.; Li, M.; Han, J.-B.; Song, H.; Liu, H.; Tang, J. Graphene Doping Improved Device Performance of Znmgo/Pbs Colloidal Quantum Dot Photovoltaics. *Adv. Funct. Mater.* **2016**, *26*, 1899−1907.
(43) Li, L.; Li, W.; Ma, C.; Yang, H.; Ge, S.; Yu, J. Paper-Based Electrochemiluminescence Immunodevice for Carcinoembryonic Antigen Using Nanoporous Gold-Chitosan Hybrids and Graphene Quantum Dots Functionalized Au@Pt. *Sens. Actuators, B* **2014**, *202*, 314−322.
(44) Suzuki, N.; Wang, Y.; Elvati, P.; Qu, Z. B.; Kim, K.; Jiang, S.; Baumeister, E.; Lee, J.; Yeom, B.; Bahng, J. H.; Lee, J.; Violi, A.; Kotov, N. A. Chiral Graphene Quantum Dots. *ACS Nano* **2016**, *10*, 1744−1755.
(45) Li, Y.; Zhao, Y.; Cheng, H.; Hu, Y.; Shi, G.; Dai, L.; Qu, L. Nitrogen-Doped Graphene Quantum Dots with Oxygen-Rich Functional Groups. *J. Am. Chem. Soc.* **2012**, *134*, 15−8.
(46) Sun, R.; Wang, Y.; Ni, Y.; Kokot, S. Graphene Quantum Dots and the Resonance Light Scattering Technique for Trace Analysis of Phenol in Different Water Samples. *Talanta* **2014**, *125*, 341−346.
(47) Zhang, P.; Zhao, X.; Ji, Y.; Ouyang, Z.; Wen, X.; Li, J.; Su, Z.; Wei, G. Electrospinning Graphene Quantum Dots into a Nanofibrous Membrane for Dual-Purpose Fluorescent and Electrochemical Biosensors. *J. Mater. Chem. B* **2015**, *3*, 2487−2496.
(48) Wang, L.; Sun, J.; Song, R.; Yang, S.; Song, H. Hybrid 2d-0d Graphene-Vn Quantum Dots for Superior Lithium and Sodium Storage. *Adv. Energy Mater.* **2016**, *6*, No. 1502067.
(49) Su, Z.; Shen, H.; Wang, H.; Wang, J.; Li, J.; Nienhaus, G. U.; Shang, L.; Wei, G. Motif-Designed Peptide Nanofibers Decorated with Graphene Quantum Dots for Simultaneous Targeting and Imaging of Tumor Cells. *Adv. Funct. Mater.* **2015**, *25*, 5472−5478.
(50) Zhang, C.; Cui, Y.; Song, L.; Liu, X.; Hu, Z. Microwave Assisted One-Pot Synthesis of Graphene Quantum Dots as Highly Sensitive Fluorescent Probes for Detection of Iron Ions and Ph Value. *Talanta* **2016**, *150*, 54−60.
(51) Zhou, Y.; Qu, Z. B.; Zeng, Y.; Zhou, T.; Shi, G. A Novel Composite of Graphene Quantum Dots and Molecularly Imprinted Polymer for Fluorescent Detection of Paranitrophenol. *Biosens. Bioelectron.* **2014**, *52*, 317−323.
(52) Wang, S.; Chen, Z.-G.; Cole, I.; Li, Q. Structural Evolution of Graphene Quantum Dots During Thermal Decomposition of Citric Acid and the Corresponding Photoluminescence. *Carbon* **2015**, *82*, 304−313.

DOI: 10.1021/acsami.7b05569
ACS Appl. Mater. Interfaces XXXX, XXX, XXX−XXX

(53) Štengl, V.; Bakardjieva, S.; Henych, J.; Lang, K.; Kormunda, M. Blue and Green Luminescence of Reduced Graphene Oxide Quantum Dots. *Carbon* **2013**, *63*, 537−546.
(54) Qin, H.; Gong, T.; Jin, Y.; Cho, Y.; Shin, C.; Lee, C.; Kim, T. Near-Uv-Emitting Graphene Quantum Dots from Graphene Hydrogels. *Carbon* **2015**, *94*, 181−188.
(55) Tsai, K.-A.; Hsu, Y.-J. Graphene Quantum Dots Mediated Charge Transfer of Cdse Nanocrystals for Enhancing Photoelectrochemical Hydrogen Production. *Appl. Catal., B* **2015**, *164*, 271−278.
(56) Song, L.; Shi, J.; Lu, J.; Lu, C. Structure Observation of Graphene Quantum Dots by Single-Layered Formation in Layered Confinement Space. *Chem. Sci.* **2015**, *6*, 4846−4850.
(57) Xu, X.; Bao, Z.; Zhou, G.; Zeng, H.; Hu, J. Enriching Photoelectrons Via Three Transition Channels in Amino-Conjugated Carbon Quantum Dots to Boost Photocatalytic Hydrogen Generation. *ACS Appl. Mater. Interfaces* **2016**, *8*, 14118−14124.
(58) Long, R.; Casanova, D.; Fang, W. H.; Prezhdo, O. V. Donor-Acceptor Interaction Determines the Mechanism of Photoinduced Electron Injection from Graphene Quantum Dots into Tio2: Pi-Stacking Supersedes Covalent Bonding. *J. Am. Chem. Soc.* **2017**, *139*, 2619−2629.
(59) Zhu, S.; Shao, J.; Song, Y.; Zhao, X.; Du, J.; Wang, L.; Wang, H.; Zhang, K.; Zhang, J.; Yang, B. Investigating the Surface State of Graphene Quantum Dots. *Nanoscale* **2015**, *7*, 7927−7933.
(60) Wang, C. C.; Lu, S. Y. Carbon Black-Derived Graphene Quantum Dots Composited with Carbon Aerogel as a Highly Efficient and Stable Reduction Catalyst for the Iodide/Tri-Iodide Couple. *Nanoscale* **2015**, *7*, 1209−1215.
(61) Eda, G.; Lin, Y. Y.; Mattevi, C.; Yamaguchi, H.; Chen, H. A.; Chen, I. S.; Chen, C. W.; Chhowalla, M. Blue Photoluminescence from Chemically Derived Graphene Oxide. *Adv. Mater.* **2010**, *22*, 505−509.
(62) Huang, S.; Qiu, H.; Zhu, F.; Lu, S.; Xiao, Q. Graphene Quantum Dots as on-Off-on Fluorescent Probes for Chromium(Vi) and Ascorbic Acid. *Microchim. Acta* **2015**, *182*, 1723−1731.
(63) Wang, F.; Gu, Z.; Lei, W.; Wang, W.; Xia, X.; Hao, Q. Graphene Quantum Dots as a Fluorescent Sensing Platform for Highly Efficient Detection of Copper(Ii) Ions. *Sens. Actuators, B* **2014**, *190*, 516−522.
(64) Wang, C.; Xu, Z.; Cheng, H.; Lin, H.; Humphrey, M. G.; Zhang, C. A Hydrothermal Route to Water-Stable Luminescent Carbon Dots as Nanosensors for Ph and Temperature. *Carbon* **2015**, *82*, 87−95.
(65) Liu, J.-H.; Anilkumar, P.; Cao, L. I.; Wang, X. I. N.; Yang, S.-T.; Luo, P. G.; Wang, H.; Lu, F.; Meziani, M. J.; Liu, Y.; Korch, K.; Sun, Y.-P. Cytotoxicity Evaluations of Fluorescent Carbon Nanoparticles. *Nano LIFE* **2010**, *01*, 153−161.
(66) Zhang, F.; Liu, F.; Wang, C.; Xin, X.; Liu, J.; Guo, S.; Zhang, J. Effect of Lateral Size of Graphene Quantum Dots on Their Properties and Application. *ACS Appl. Mater. Interfaces* **2016**, *8*, 2104−2110.
(67) Wang, Z.; Yu, J.; Zhang, X.; Li, N.; Liu, B.; Li, Y.; Wang, Y.; Wang, W.; Li, Y.; Zhang, L.; Dissanayake, S.; Suib, S. L.; Sun, L. Large-Scale and Controllable Synthesis of Graphene Quantum Dots from Rice Husk Biomass: A Comprehensive Utilization Strategy. *ACS Appl. Mater. Interfaces* **2016**, *8*, 1434−1439.
(68) Xu, Z. Q.; Lan, J. Y.; Jin, J. C.; Dong, P.; Jiang, F. L.; Liu, Y. Highly Photoluminescent Nitrogen-Doped Carbon Nanodots and Their Protective Effects against Oxidative Stress on Cells. *ACS Appl. Mater. Interfaces* **2015**, *7*, 28346−28352.

DOI: 10.1021/acsami.7b05569
ACS Appl. Mater. Interfaces XXXX, XXX, XXX−XXX